ES Materials and Manufacturing
DOI: https://dx.doi.org/10.30919/esmm5f727

Preparation and Response Characteristics of Acoustic Emission Sensors with Different Matching Layers

Mei Cao,[1] Dandan Sun,[1] Haoran Li,[1] Deli Lou,[2] Fan Yang,[3] Peng Du,[1] Dongyu Xu[4,*] and Shoude Wang[1,*]

Abstract

Acoustic emission (AE) sensor for concrete structure damage monitoring was designed and prepared by using piezoelectric ceramics as components and aluminum and aluminum oxide as matching layers. The conductivity frequency diagram before and after piezoelectric elements packaging was studied as well as the AE response characteristics after ball impact and pencil lead break (PLB). The conductance frequency diagram indicate that the dominant resonant frequency is reduced. The ball hitting research results show that the amplitude, hit counts and rising time, produced by rubber and steel ball impact are basically the same, nevertheless, the energy produced by steel ball impact is higher than that of the rubber ball, which is about 20 times of the rubber ball. AE response amplitude and hit counts caused by the same kind of balls are basically same, but the rising time and energy in concrete slab are about 0.1 times of those in aluminum and steel slabs. The PLB results show that there exist a highest receiving sensitivity for the AE sensor made of aluminum matching layer in concrete slab, and made of aluminum oxide matching layer in aluminum and steel slab, respectively. The attenuation coefficient of sensor is the largest in concrete slab.

Keywords: Acoustic emission; Piezoelectric; Sensor; Concrete; Aluminum.
Received: 9 March 2022; Revised: 29 March 2022; Accepted: 27 May 2022.
Article type: Research article.

1. Introduction

The bearing capacity and health status of in-service concrete structures will deteriorate in varying degree with service time as a result of the bad service environment and complex load action forms.[1-4] Therefore, grasping the damage location, degree and service state of concrete structures or stressed components plays a vital role in evaluating safety and predicting residual life.[5-7]

Acoustic emission (AE) technology is widely used in the concrete structure health monitoring filed, realizing real-time dynamic monitoring of damage location and damage degree of concrete materials.[8-12] Chen *et al*.[13] developed piezoelectric lead zirconate titanate (PZT) nanofiber AE sensors with small size, high flexibility and high sensitivity to monitor small-size structures, curving surface and even living cells. Dong *et al*.[14] introduced the application of a new cement-based piezoelectric ceramic sensor in static load stress monitoring of reinforced concrete beams. The results show that the electromechanical response of the sensor embedded in the reinforced concrete beam under various load conditions is linear. Chen *et al*.[15] systematically review the recent progress on conductive polymer composites (CPCs)-based temperature sensors, as well as their mechanisms and applications in different fields. Aggelis *et al*.[16] recorded the AE activity in the fatigue test of metal specimens, indicating that the damage mechanism and the ultimate life of materials under fatigue can be predicted.

In AE detection technology, sensor is the core device to receive signal, which is usually composed of sensing element, matching layer, backing layer and packaging shell. The matching layer plays an important role in realizing acoustic impedance, matching and improving sensor sensitivity and acoustic transmittance. According to the direct time domain analysis of ultrasonic transmission and reflection characteristics, Kim *et al*.[17] developed a new transducer performance evaluation parameter and optimized the optimal acoustic impedance of the matching layer. Bian *et al*.[18] proposed an acoustic gradient impedance matching layer

[1] *Shandong Key Laboratory of Building Materials Preparation and Testing Technology, University of Jinan, Jinan, 250022, China.*
[2] *Jinan Sijian Construction Group Co., LTD, Jinan, 250031, China.*
[3] *Guangxin Testing and Certification Group Co., LTD, Jinan, 250031, China.*
[4] *School of Civil Engineering and Architecture, Linyi University, Linyi, 276000, P. R. China.*
**Email:* xuy_sha@163.com (S. Wang); xudongyu@lyu.edu.cn (D. Xu)

material, filling a specific binary mixture into the conical cavity structure generated by three dimension (3D) accurate printing, and the sensor emission voltage response bandwidth (-3 dB) reaches 110%. Manh *et al*.[19] proposed a new method for manufacturing multi-layer matching layer of 15 MHz piezoelectric ultrasonic transducer.

At present, lots of tests about AE detection technology and sensors were carried out, but a few of studies on AE sensors suitable for concrete structure damage detection were reported. In this paper, an AE sensor for concrete damage monitoring is prepared by using piezoelectric ceramic as sensing element and aluminum and aluminum oxide as matching layer respectively. The influence of different matching layers on the performance of AE sensor was studied, and its application in ball impact and pencil lead break (PLB) of AE detection was discussed.

2. Preparation of AE sensor

2.1 AE detection principle

When the elastic wave from the AE source reaches the medium surface, leading to surface displacement of the transmitted medium. The AE sensor detects the surface displacement and converts the mechanical vibration of the material into electrical signals.[20,21] These electrical signals are amplified, processed and recorded by the AE acquisition system, and the AE detection processing is shown in Fig. 1.

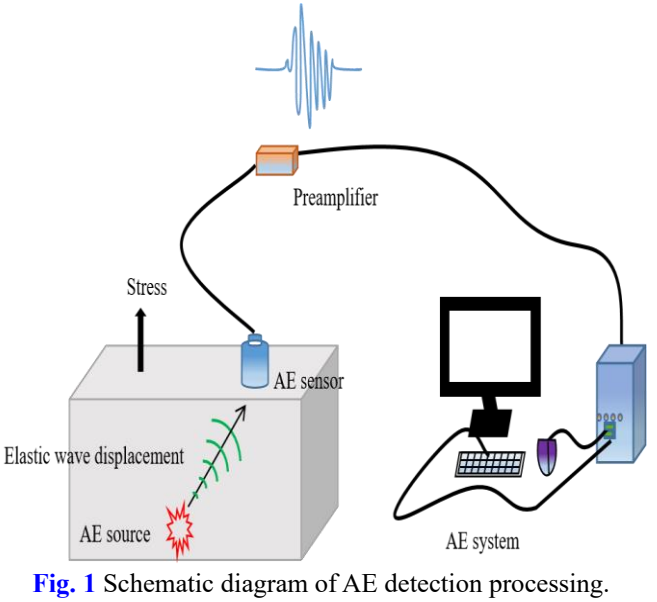

Fig. 1 Schematic diagram of AE detection processing.

2.2 Structure design and preparation of AE sensor

AE sensor is a kind of transducer that converts the surface vibration of the test piece caused by AE wave into voltage signal. As a sensitive element to receive the signal, it plays a vital role as a bridge in the AE system. Fig. 2 is cross section of AE sensor. Here, PZT was used as the main sensing element. The matching layer connects the sensing element with the detected object, improving the projection rate of sound wave and protecting the piezoelectric element. The backing layer can reduce the secondary piezoelectric effect caused by the sound wave passing through the piezoelectric element returning to the piezoelectric crystal due to the reflection of the interface.

PZT-5 piezoelectric ceramics of 40 × 40 × 8 mm were used to fabricate the AE sensors, whose main performance parameters were shown in Table 1.

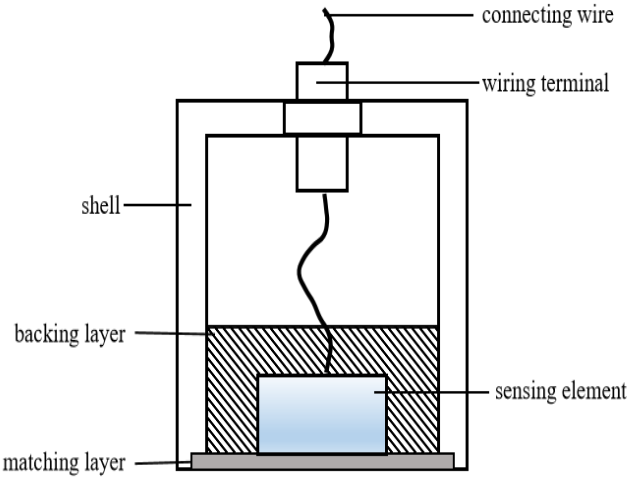

Fig. 2 Cross section of AE sensor.

Table 1. Main performance parameters of piezoelectric ceramics.

Density ρ (10^3kg·m^{-3})	Dielectric constant ε_r	Piezoelectric strain constant d_{33}/(pC·N^{-1})	Piezoelectric voltage constant g_{33}/(10^{-3}V·m·N^{-1})
7.4	1500	440	32.6

The acoustic impedance of piezoelectric ceramics was about 30.5 MRayl, and that of the concrete was about 9.5 MRayl. According to the basic acoustics principle,[22] the calculated acoustic impedance of the best matching layer was 17.02 MRayl. Therefore, aluminum and aluminum oxide were used as matching layers to prepare AE sensors in this paper. Firstly, the piezoelectric ceramic was bonded to the matching layer and the wire was welded. Secondly, epoxy resin and tungsten powder were selected as the backing layer, in which the backing layer was composed of epoxy resin main agent: curing gent: tungsten powder = 4 : 1 : 8. Finally, the matching layer, piezoelectric ceramic and backing layer were encapsulated in the shell to obtain AE sensors with different matching layers, which were termed as L_a (the AE sensor of aluminum matching layer) and L_b (AE sensor of aluminum oxide matching layer), respectively.

2.3 Electrical impedance and AE response test

The conductance parameters of piezoelectric element and AE sensor were measured by impedance analyzer (Agilent 4294A, USA). The test frequency ranges from 50 kHz to 300 kHz. The resonant, antiresonant frequencies of piezoelectric element and AE sensor were obtained according to the conductance frequency diagram.

The steel and rubber balls (7 mm) were selected to fall from different heights (20 cm, 15 cm and 10 cm) to impact the tested

pieces (aluminum slab 500 × 500 × 2 mm, concrete slab 300 × 300 × 30 mm, steel slab 600 × 600 × 2 mm), as shown in Fig. 3. The WSα SNAE30 sensors (PAC, USA), L_a and L_b were placed on the tested pieces with equal distances, respectively. The distance between the falling position of the ball and the three sensors were equal, the sensor and the tested pieces were connected with Vaseline as coupling agent, the AE signal was collected with an acoustic emitter (PAC micro-II, USA), the acquisition threshold was 40 dB, and the amplification factor of the charge amplifier (PAC Model: 2 / 4 / 6, USA) was 40 dB.

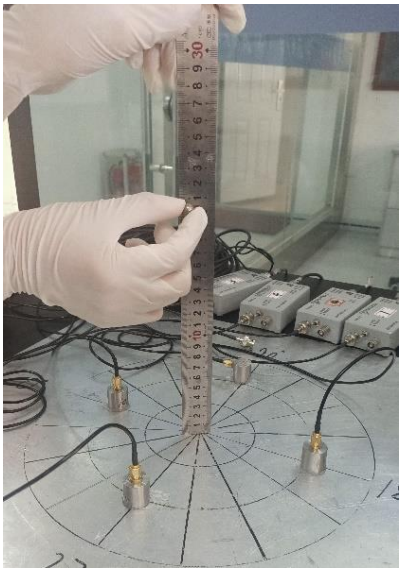

Fig. 3 Ball hitting experiment in steel slab.

The Nielsen Hsu pencil lead break (PLB) method with 0.5 mm pencil core was simulated at the center of the circle,[23,24] PLB was carried out along the surface of the tested pieces at an angle of 30º, the lead core was extended by 2.5 mm, and the AE system was used to collect the signals. The aluminum, concrete and steel slab were used as tested pieces, and the distance between the pencil lead and the sensors was equal. Fig. 4 is schematic diagram of PLB.

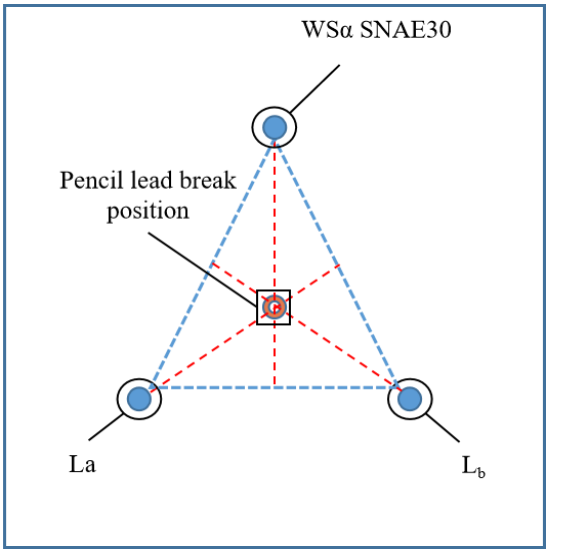

Fig. 4 Schematic diagram of PLB.

3. Result analysis and discussion

3.1 Frequency characteristics

The conductivity frequency diagram of AE sensors with different matching layers in different packaging states is shown in Fig. 5. It can be found that, compared with the conductivity frequency diagram of piezoelectric ceramics before packaging, the main resonance frequency and corresponding conductivity of the encapsulated AE sensor are reduced. After pasting the matching layer, the resonance frequency of the AE sensor moves to low frequency, the bandwidth is extended from 130-150 kHz to 110-150 kHz, and the working bandwidth of the sensor is significantly extended.

3.2 AE impact response characteristics

In order to compare the AE impact response characteristics of different AE sensors, steel ball is dropped from a height of 20 cm to impact the steel slab. Different AE sensors is used to record the AE signals, and the time domain diagram is shown in Fig. 6(a), the frequency domain diagram is obtained by Fourier transform, as shown in Fig. 6(b).

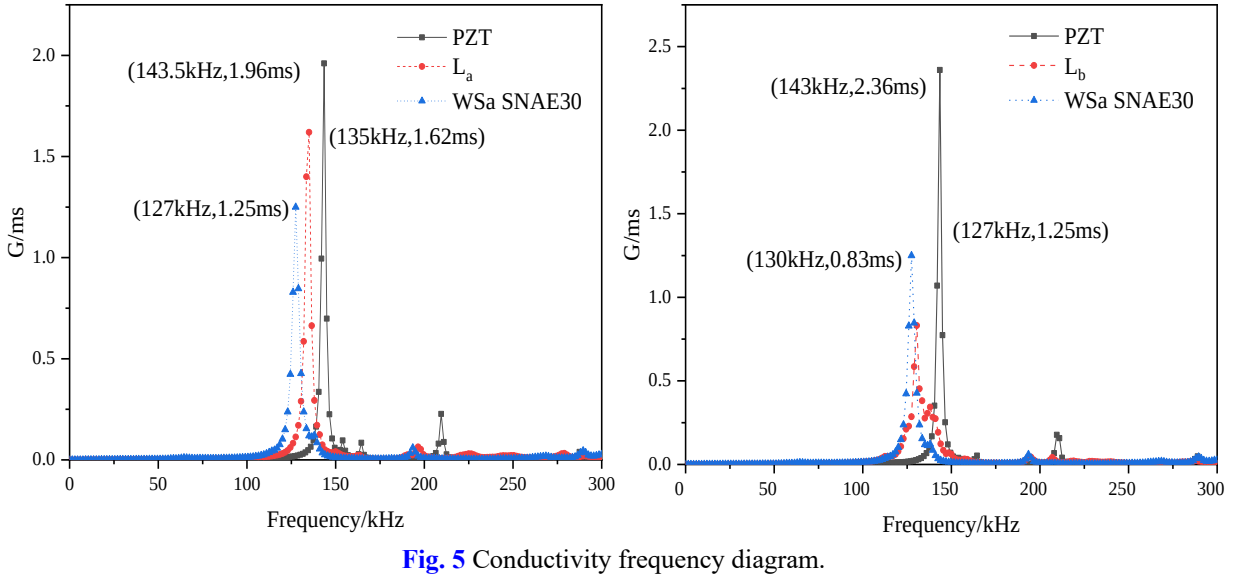

Fig. 5 Conductivity frequency diagram.

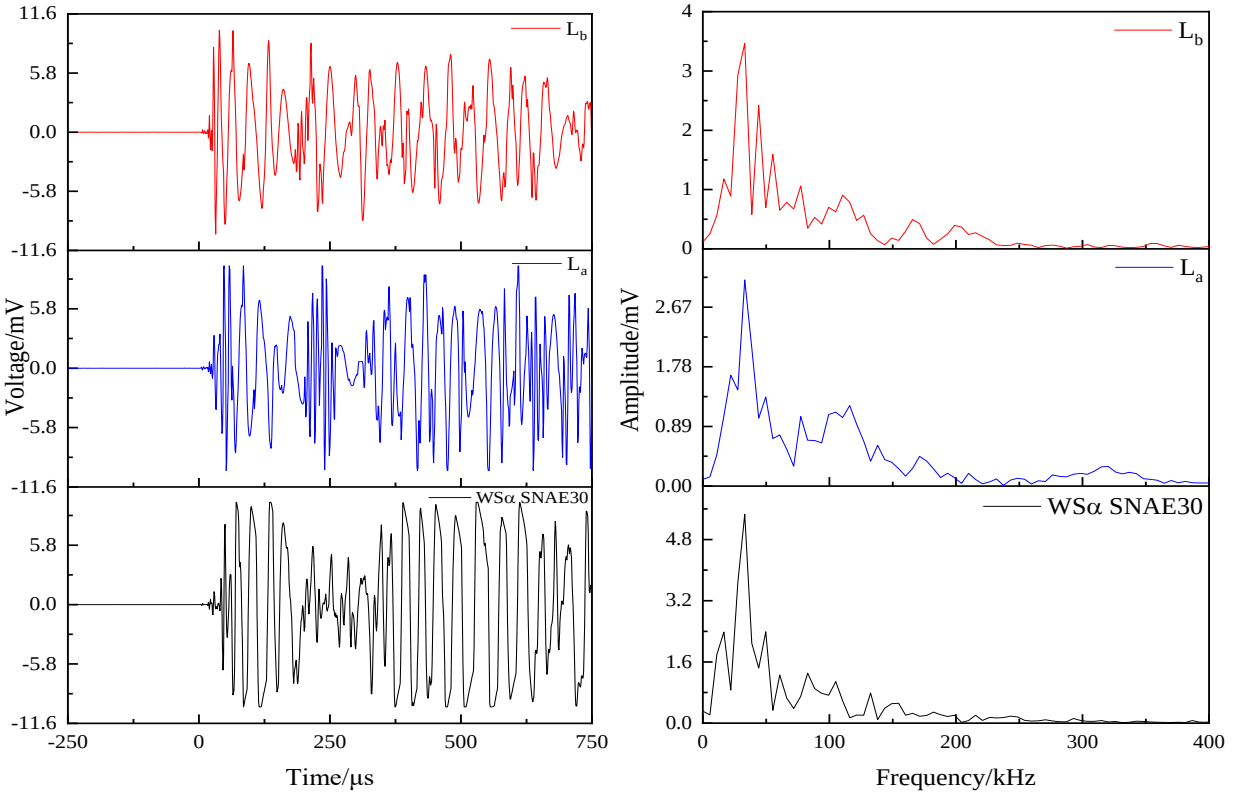

(a) Time domain diagram (b) Frequency domain diagram

Fig. 6 Time and frequency domain diagrams of AE signal by steel ball impact.

According to Fig. 6, the time domain peak-to-peak value of different sensors is similar, which is about 8.7 mV. The corresponding frequency of different sensors' dominant frequency peak is about 25 kHz. The response amplitude of the reference sensor's dominant peak frequency is 5.4 mV, and those of L_a and L_b are 3.1 mV and 3.4 mV, respectively. From the above analysis, it can be seen that L_a and L_b have good consistency.

3.2.1 Effects of impactors on AE response

Figure 7 shows the AE characteristic parameters of steel ball impacting different media. It can be found that there are

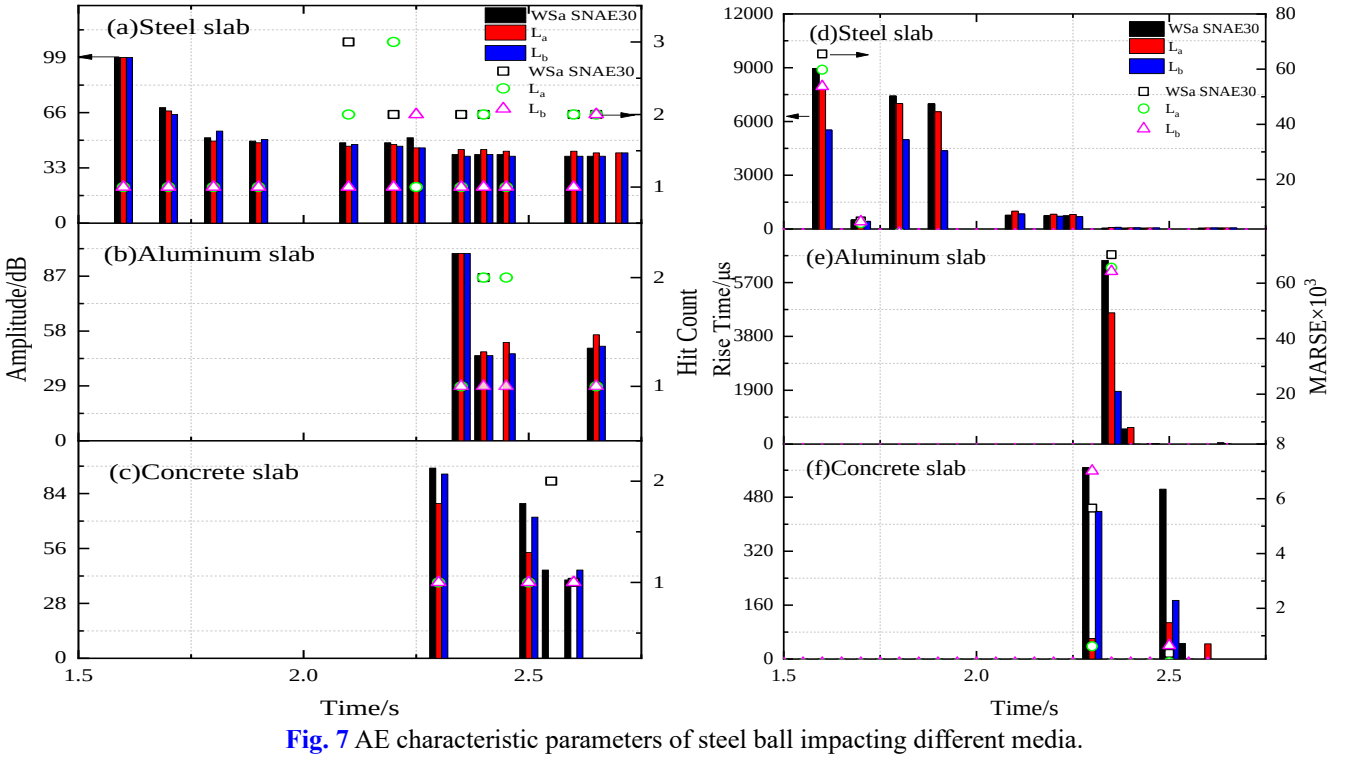

Fig. 7 AE characteristic parameters of steel ball impacting different media.

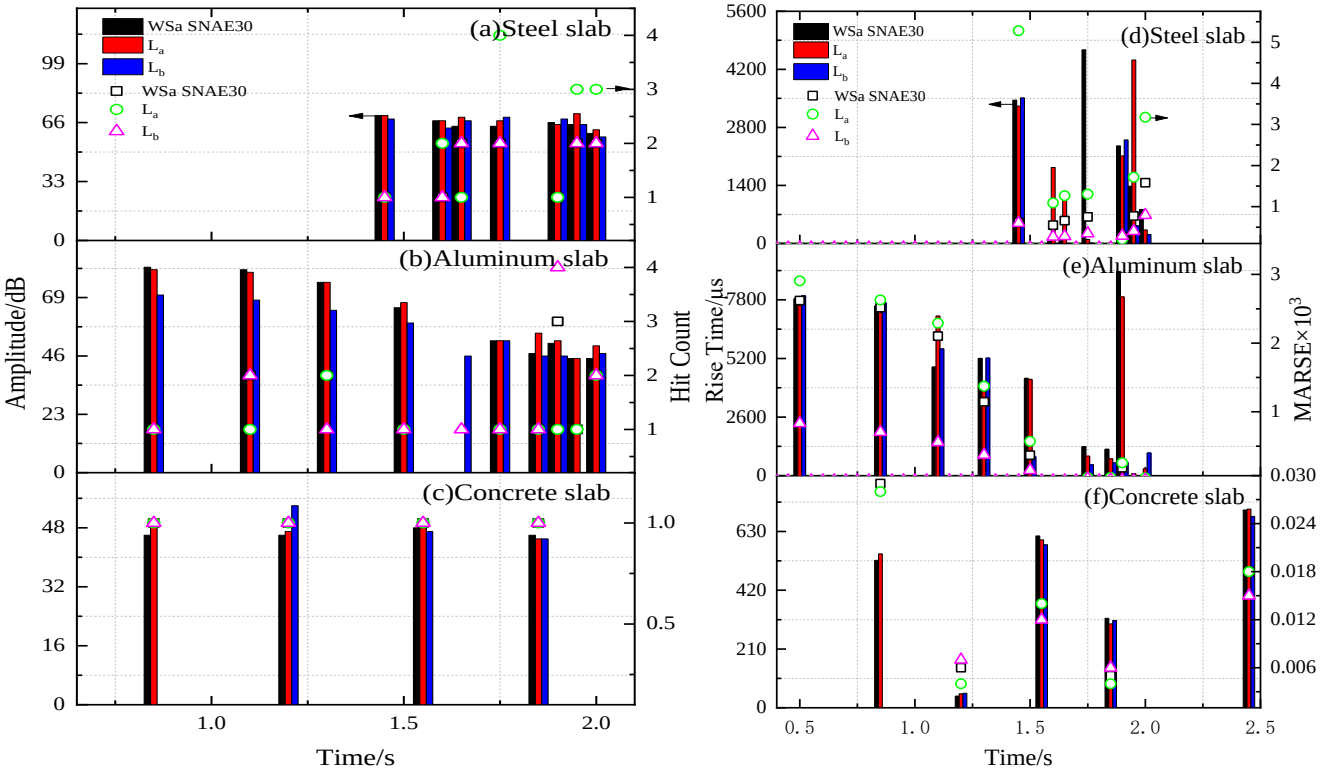

Fig. 8 AE characteristic parameters of rubber ball impacting different media.

impacting, rebounding and rolling signals after steel ball hit different media. The impact signal generated during the first impact has a high amplitude, rising time and energy received by the sensor, but rebounding and rolling signals are decreased significantly. And the AE signals are produced by the steel ball impacting on concrete slab are less. The rising time and energy of the AE signal in concrete slab are about 0.1 times of those in aluminum and steel slab. This is because that more amplitude is caused by the steel ball rebounding and rolling on different media. At the same time, the propagation distance of stress wave caused by steel ball rebounding and rolling is different, resulting in the rising time and energy caused by impacting of same medium are different.

Figure 8 shows the AE characteristic parameters of the rubber ball impacting different media. It can be found that there are impacting and rebounding signals after the rubber ball impacts different media, and with the increase of the rebound times, the amplitude received by sensors are decreased. When impacting the concrete slab, rising time and energy of sensors received are 0.01 times of aluminum and steel slab. It is possible that the concrete is a composite material with internal non-uniformity, the AE signal generated by impacting concrete slab attenuates rapidly and the slab is thick, resulting in small acoustic wave velocity and AE signal.

3.2.2 Effects of impact heights on AE response

Although the response of AE characteristics parameters of different sensors in different media are different, which have good response to impacting events. In order to verify the consistency of sensors, the AE characteristics of falling from different heights are studied. Because the steel and rubber ball have good AE signal response, the impact of steel ball on aluminum slab was studied in this experiment.

Figure 9 shows AE characteristic parameters of steel balls impacting steel slab from different heights. It can be found that when the steel ball falls from 20 cm, there are impacting, rebounding and rolling signals. When it falls from 15 cm and 10 cm, there are impacting and rolling signals, and the amplitude, energy and rising time of the impact signal were large. Due to the existence of air friction resistance, the bounce height and AE signal are small. The amplitudes received by the three sensors from different heights have slight differences. When the falling height becomes lower, the number of AE signals increases, and each sensor can effectively record the AE signals generated by impact.

The above analysis of AE characteristic parameters shows that the response of AE characteristic parameters of sensors in different matching layers is different. The AE signal generated by steel ball impact is greater than that of rubber ball. The signal generated by steel ball (rubber ball) impact on concrete slab is lower than that of the steel and aluminum slabs. Each sensor has good response ability to impact events, and it can effectively record the signal generated by impact.

3.3 AE response on PLB

3.3.1 Time and frequency diagrams analysis

Figure 10 shows the time and frequency domain diagrams of the PLB signal received by the AE sensor on the concrete slab. It can be found that the time domain waveform peak and sensitivity of L_b is the highest, and the reference sensor is the

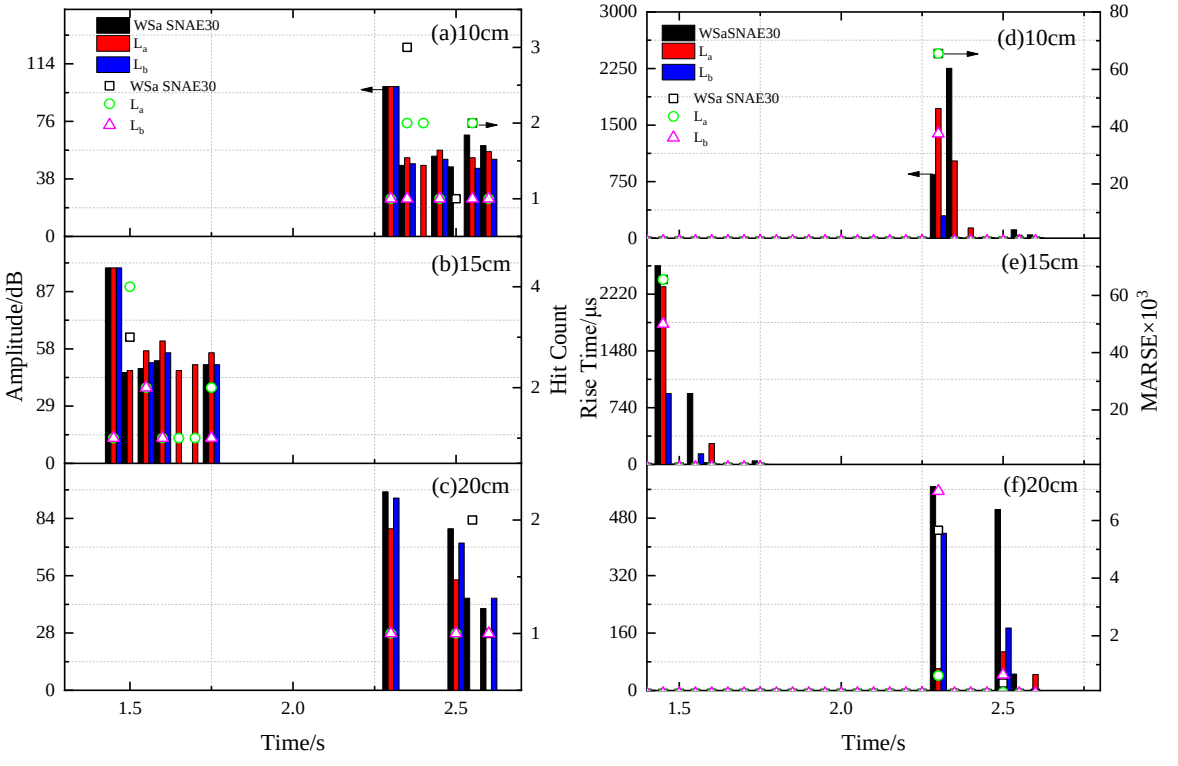

Fig. 9 AE characteristic parameters of steel balls impacting steel slab from different heights.

lowest. The dominant frequency of L_a and L_b is similar, which is about 175 kHz, and the reference sensor is 100 kHz. At the same time, compared with the reference sensor and L_a, the dominant frequency amplitude of L_b is larger, which is 0.77 mV. In the frequency domain diagram, the decrease of -6 dB in the maximum amplitude of the sensor is regarded as the bandwidth of the sensor. It can be found that the bandwidth of the reference sensor and L_a is wide, nevertheless, that of L_b is narrow.

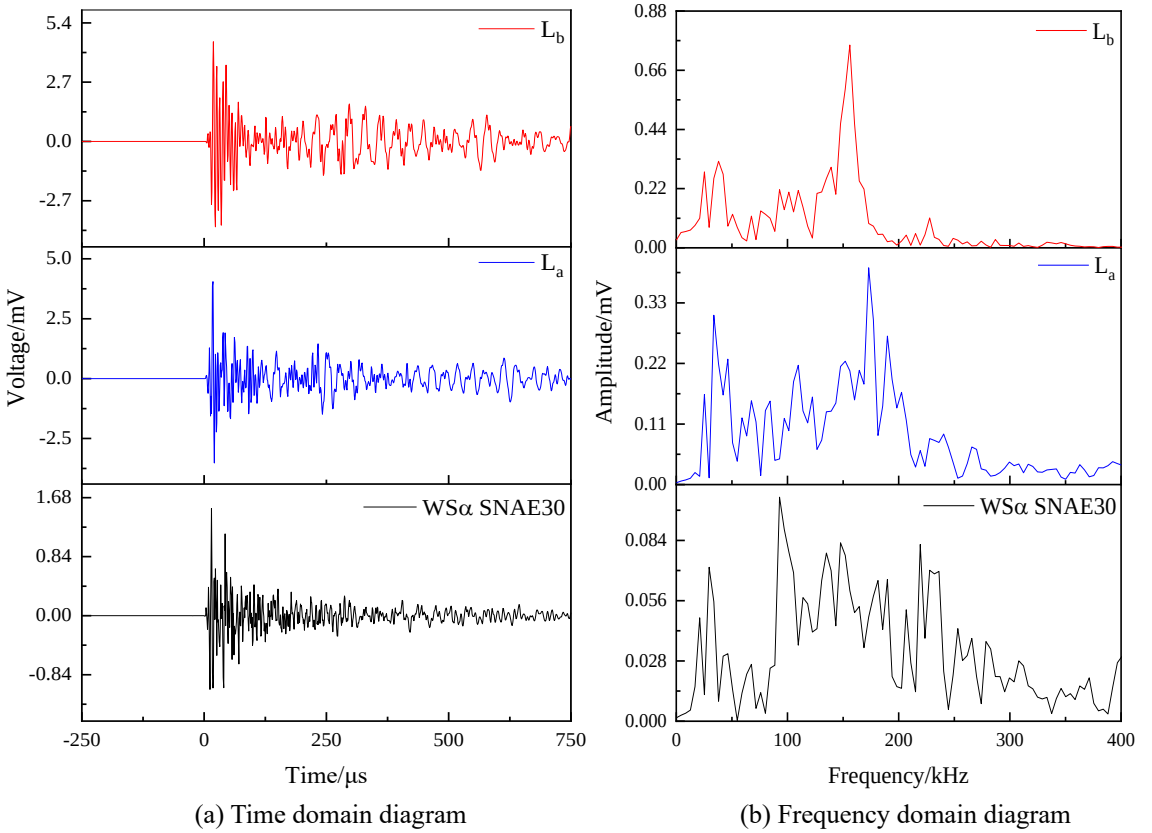

(a) Time domain diagram (b) Frequency domain diagram

Fig. 10 Time and frequency domain diagrams of AE sensor receiving PLB signal in concrete slab.

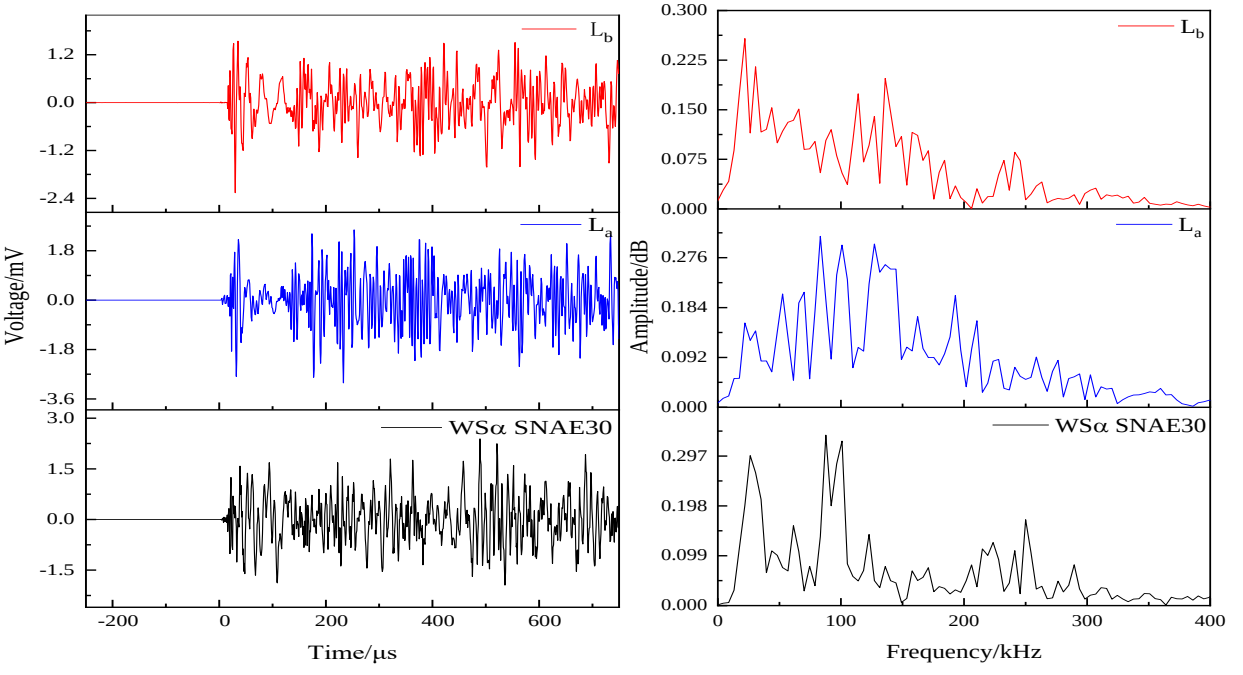

(a) Time domain diagram (b) Frequency domain diagram

Fig. 11 Time and frequency domain diagrams of AE sensor receiving PLB signal in aluminum slab.

Figure 11 shows the time and frequency domain diagram of AE sensor receiving PLB signal in aluminum slab. It can be found that the time domain waveform peak and sensitivity of L_a is the highest, and L_b is the lowest. The dominant frequency of L_a and the reference sensor is similar about 100 kHz, and that of the L_b is 25 kHz. The dominant frequency amplitude of reference sensor is highest, and L_b is lowest, which is about 0.26 mV. And the bandwidth of different sensors is similar.

Figure 12 shows the time and frequency domain diagrams of AE sensor receiving PLB signal in steel slab. It can be found that the time domain waveform peak and sensitivity of L_a is the highest, and the reference sensor is the lowest. The dominant frequency of L_a and L_b is similar, which is about 150 kHz, and the reference sensor is 100 kHz. The dominant frequency amplitude of L_a is the highest, which is about 0.016 mV, and the bandwidths of L_a and L_b are similar. The time domain diagrams of the signals received by different sensors when PLB on the same media have a high similarity as a whole, however, the same sensor on different media is quite different. The receiving sensitivity of L_b in the concrete slab is the

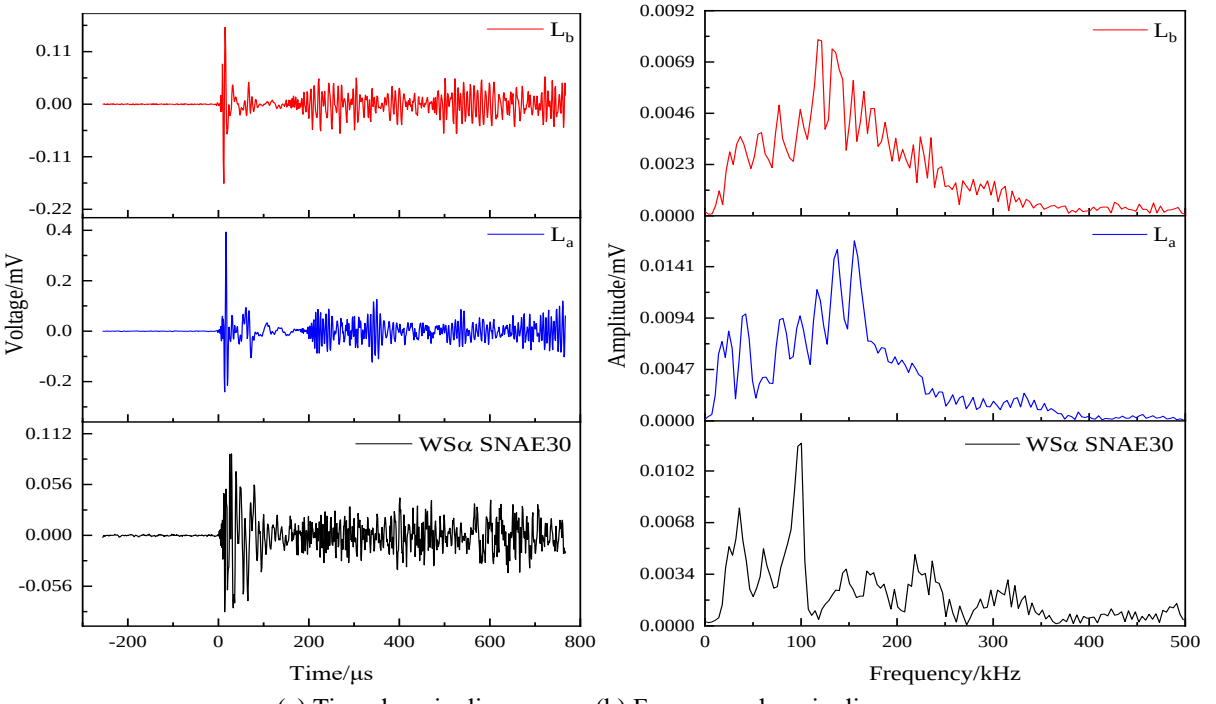

(a) Time domain diagram (b) Frequency domain diagram

Fig. 12 Time and frequency domain diagrams of AE sensor receiving PLB signal in steel slab.

highest, and that of L_a is higher than L_b in aluminum and steel slab. Due to the different sound velocity and density of materials, the acoustic impedance is different, resulting in different signals received by the sensors.

3.3.2 AE attenuation characteristics on different media

The attenuation of sound wave refers to the phenomenon that the intensity of sound wave decreases gradually with the increase of propagation distance. The AE sensors were placed on aluminum, concrete and steel slab, respectively. At the distance of 0 cm, 5 cm, 10 cm, 15 cm, 20 cm, 25 cm, 30 cm, 35 cm and 40 cm away from the sensor, three times of PLB experiments were carried out, respectively, as shown in Fig. 13. Average values were obtained, and graphs were drawn.

It can be seen from Fig. 14, as the measuring points are far away from the sensor, the amplitude and energy received by the AE sensors generally show a trend of attenuation. The farther the distance is, the slower the attenuation is. It might be that the influence of noises is eliminated during AE parameters are set. The AE signal was recorded when it is higher than the threshold value. It can be seen that the energy received by the AE sensor on the concrete slab is low and attenuates rapidly.

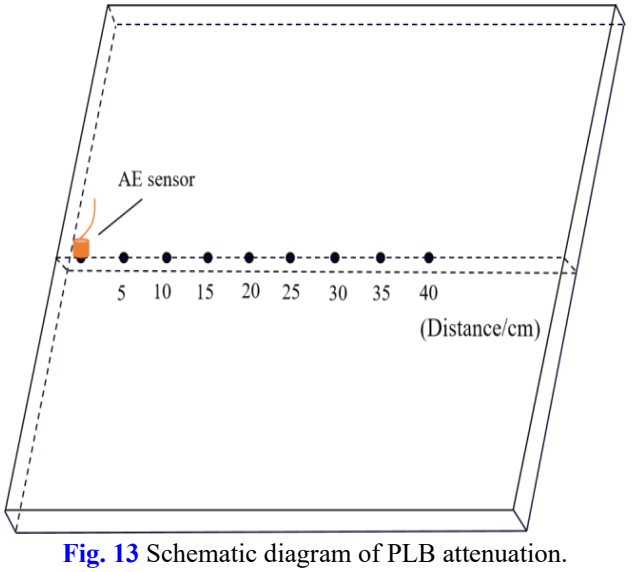

Fig. 13 Schematic diagram of PLB attenuation.

The formula of sound pressure attenuation with distance is as follows[25]:

$$P(x) = P_0 e^{-\alpha x} \quad (1)$$

where P_0 is the sound pressure of sound source, P(x) is the sound pressure of distance, and α is the amplitude attenuation coefficient. The energy of the signal is as following equation:

$$E(x) = E_0 e^{-\alpha_E x} \quad (2)$$

where E_0 is the sound source energy, E(x) is the AE energy after the propagation distance, and α_E is the energy attenuation coefficient. The energy of AE wave in time is shown in following equation:

$$E_t = \int_0^1 P^2(t)dt \quad (3)$$

By combining (1) - (3), the energy attenuation coefficient α_E is twice the amplitude attenuation coefficient α, that is:

$$\alpha_E = 2\alpha \quad (4)$$

Therefore, according to the linear relationship, the energy attenuation coefficient was studied in this paper. By fitting the energy curves of sensors received in different media according to the formula, the fitting energy attenuation coefficient and fitting degree R^2 can be obtained, as shown in Table 2.

Table 2. Attenuation coefficient on different media.

AE sensor	Aluminum slab		Steel slab		Concrete slab	
	R^2	α_E	R^2	α_E	R^2	α_E
WSα SNAE30	0.00862	0.82	0.02397	0.83	0.0722	0.94
L_a	0.00788	0.88	0.02183	0.86	0.06485	0.92
L_b	0.00832	0.88	0.0106	0.89	0.06745	0.91

It can be found that the values of each fitting degree show a negative exponential correlation with the attenuation of energy with distance below the confidence interval of 95%. The energy attenuation coefficient of different sensors on the same media is similar, but the same sensor on different media is quite different. At the same time, it can be found that the attenuation coefficient of concrete slab is the highest, aluminum slab is the lowest, the maximum attenuation coefficient of concrete slab is 0.0722, 0.06485 and 0.06745, respectively, and the minimum attenuation coefficient of aluminum slab is 0.00862, 0.00788 and 0.00832, respectively. This may be because the concrete is a non-uniform material. Due to the action of internal bubbles and aggregates, the sound wave is easy to scatter and refract after passing through a variety of media, so that the elastic wave generated by the PLB experiment diffuses in the form of micro particle vibration during the propagation of concrete. There are different of particle sizes and shapes of aggregates, lead to the different friction damping and attenuation coefficient between particles. The greater attenuation coefficient is, the faster attenuation speed is.

4. Conclusion

In this paper, AE sensors with different matching layers were prepared. Compared with PZT ceramics, the resonant frequency of the AE sensor moves to low frequency after pasting the matching layer, and the working bandwidth of the sensor is extended obviously. The sensors with different matching layers have different acoustic impedance matching on different media. L_a and L_b have the highest receiving sensitivity on concrete slab and aluminum and steel slab, respectively. The results show that the attenuation coefficient of PLB in concrete slab is the highest, and aluminum slab is the lowest. The test results also show that the AE sensors with different matching layers have good signal receiving ability and AE characteristic response, and are suitable for concrete monitoring.

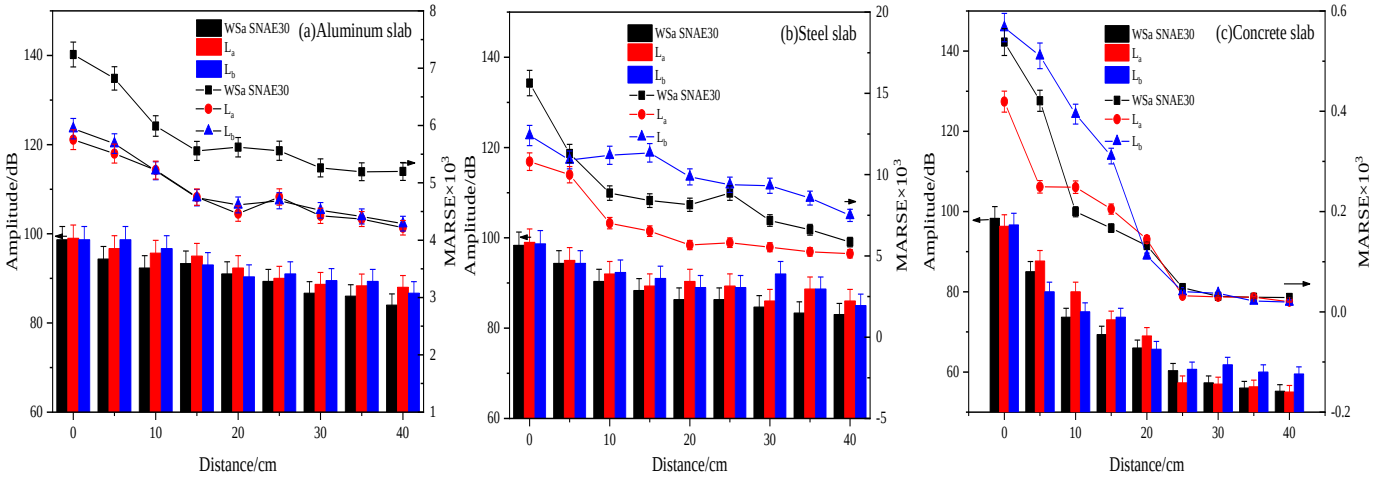

Fig. 14 AE signal attenuation curve.

Acknowledgement

This study was supported by the National Key Research and Development Program of China (No.2017YFE0120900).

Conflict of Interest

There is no conflict of interest.

Supporting Information

Not applicable.

References

[1] J. Cui, H. Hao, Y. Shi, Study of concrete damage mechanism under hydrostatic pressure by numerical simulations, *Construction and Building Materials*, 2018, **160**, 440-449, doi: 10.1016/j.conbuildmat.2017.11.083.

[2] B. Isojeh, M. El-Zeghayar, F. J. Vecchio, Concrete damage under fatigue loading in uniaxial compression, *ACI Materials Journal*, 2017, **114**, 225-235, doi: 10.14359/51689477.

[3] A. Bagheri, A. Ajam, H. Zanganeh, Investigation of chloride ingress into concrete under very early age exposure conditions, *Construction and Building Materials*, 2019, **225**, 801-811, doi: 10.1016/j.conbuildmat.2019.07.225.

[4] B. Wang, F. Wang, Q. Wang, Damage constitutive models of concrete under the coupling action of freeze-thaw cycles and load based on Lemaitre assumption, *Construction and Building Materials*, 2018, **173**, 332-341, doi: 10.1016/j.conbuildmat.2018.04.054.

[5] P. R. Prem, A. R. Murthy, Acoustic emission monitoring of reinforced concrete beams subjected to four-point-bending, *Applied Acoustics*, 2017, **117**, 28-38, doi: 10.1016/j.apacoust.2016.08.006.

[6] Z. Zhao, C. Chen, A fuzzy system for concrete bridge damage diagnosis, *Computers & Structures*, 2002, **80**, 629-641, doi: 10.1016/s0045-7949(02)00031-7.

[7] A. V. Lavrov, V. L. Shkuratnik, Deformation-and fracture-induced acoustic emission in rocks, *Acoustical Physics*, 2005, **51**, S2-S11, doi: 10.1134/1.2133948.

[8] J. Zhang, Z. Kang, D. Hou, B. Dong, H. Ma, Wavelet power and Shannon entropy applied to acoustic emission signals for corrosion detection and evaluation of reinforced concrete, *ES Materials & Manufacturing*, 2021, **16**, 46-55, doi: 10.30919/esmm5f554.

[9] K. T. Wan, C. K. Y. Leung, Applications of a distributed fiber optic crack sensor for concrete structures, *Sensors and Actuators A: Physical*, 2007, **135**, 458-464, doi: 10.1016/j.sna.2006.09.004.

[10] A. S. Suvorov, E. M. Sokov, P. V. Artel'nyi, Numerical simulation of acoustic emission using acoustic contact elements, *Acoustical Physics*, 2014, **60**, 694-703, doi: 10.1134/s1063771014060189.

[11] D. Wells, An acoustic apparatus to record emissions from concrete under strain, *Nuclear Engineering and Design*, 1970, **12**, 80-88, doi: 10.1016/0029-5493(70)90135-4.

[12] M. Abdelrahman, M. K. ElBatanouny, P. H. Ziehl, Acoustic emission based damage assessment method for prestressed concrete structures: modified index of damage, *Engineering Structures*, 2014, **60**, 258-264, doi: 10.1016/j.engstruct.2013.12.037.

[13] X. Chen, S. Guo, J. Li, G. Zhang, M. Lu, Y. Shi, Flexible piezoelectric nanofiber composite membranes as high performance acoustic emission sensors, *Sensors and Actuators A: Physical*, 2013, **199**, 372-378, doi: 10.1016/j.sna.2013.06.011.

[14] B. Dong, Y. Liu, L. Qin, Y. Wang, Y. Fang, F. Xing, X. Chen, *in situ* stress monitoring of the concrete beam under static loading with cement-based piezoelectric sensors, *Nondestructive Testing and Evaluation*, 2015, **30**, 312-326, doi: 10.1080/10589759.2015.1046452.

[15] J. Chen, Y. Zhu, Z. Guo, A. G. Nasibulin, Recent progress on thermo-electrical properties of conductive polymer composites and their application in temperature sensors, *Engineered Science*, 2020, **12**, 13-22, doi: 10.30919/es8d1129.

[16] D. G. Aggelis, E. Z. Kordatos, T. E. Matikas, Acoustic emission for fatigue damage characterization in metal plates, *Mechanics Research Communications*, 2011, **38**, 106-110, doi: 10.1016/j.mechrescom.2011.01.011.

[17] Y.-B. Kim, New design of matching layers for high power and wide band ultrasonic transducers, *Sensors and Actuators A: Physical*, 1998, **71**, 116-122, doi: 10.1016/S0924-4247(98)00151-4.

[18] J. Bian, Y. Wang, Z. Liu, M. Shen, H. Zhao, Y. Sun, J. Zhu, Ultra-wideband underwater acoustic transducer with a gradient

impedance matching layer, *Applied Acoustics*, 2021, **175**, 107789, doi: 10.1016/j.apacoust.2020.107789.
[19] T. Manh, A.-T T. Nguyen, T. F. Johansen, L. Hoff, Microfabrication of stacks of acoustic matching layers for 15MHz ultrasonic transducers, *Ultrasonics*, 2014, **54**, 614-620, doi: 10.1016/j.ultras.2013.08.015.
[20] G. W. Rodgers, R. Welsh, L. J. King, A. J. FitzPatrick, T. B. F. Woodfield, G. J. Hooper, Signal processing and event detection of hip implant acoustic emissions, *Control Engineering Practice*, 2017, **58**, 287-297, doi: 10.1016/j.conengprac.2016.09.013.
[21] I. Ben Ammar, C. Karra, A. El Mahi, R. El Guerjouma, M. Haddar, Mechanical behavior and acoustic emission technique for detecting damage in sandwich structures, *Applied Acoustics*, 2014, **86**, 106-117, doi: 10.1016/j.apacoust.2014.04.016.
[22] S. E. Hamdi, A. Le Duff, L. Simon, G. Plantier, A. Sourice, M. Feuilloy, Acoustic emission pattern recognition approach based on Hilbert-Huang transform for structural health monitoring in polymer-composite materials, *Applied Acoustics*, 2013, **74**, 746-757, doi: 10.1016/j.apacoust.2012.11.018.
[23] R. Ernst, F. Zwimpfer, J. Dual, One sensor acoustic emission localization in plates, *Ultrasonics*, 2016, **64**, 139-150, doi: 10.1016/j.ultras.2015.08.010.
[24] G. K. Kocur, Deconvolution of acoustic emissions for source localization using time reverse modeling, *Journal of Sound and Vibration*, 2017, **387**, 66-78, doi: 10.1016/j.jsv.2016.10.021.
[25] J. Zhang, T. Fan, H. Ma, Z. Li, Monitoring setting and hardening of concrete by active acoustic method: effects of water-to-cement ratio and pozzolanic materials, *Construction and Building Materials*, 2015, **88**, 118-125, doi: 10.1016/j.conbuildmat.2015.04.010.

Author Information

Mei Cao *obtained her bachelor degree in 2018 from Shandong Jianzhu University and master degree in 2022 from University of Jinan. Her research mainly focuses on cement-based materials, acoustic emission sensors and structual health monitoring.*

Dandan Sun *obtained her bachelor degree in 2019 from Shandong Jiaotong University and master degree in 2022 from University of Jinan. Her research focuses on cement-based materials, ultrasonic sensors and nondestructive testing.*

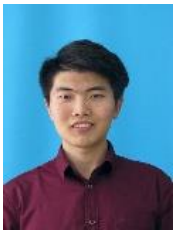

Haoran Li *obtained his bachelor degree from Shandong Jianzhu University in 2014. He is now a PhD candidate at University of Jinan. His research focus on ultrasonic monitoring and testing of cement concrete.*

Deli Lou *is a Senior Engineer in the Jinan Sijian Construction Group Co., LTD. He received his BSc at University of Jinan. His research interests are in cement and concrete materials. He has obtained 17 authorized patents.*

Fan Yang *is a Senior Engineer in the Guangxin Testing and Certification Group Co., LTD. He received his BSc at University of Jinan. His research interests are in nondestructive evaluation of materials.*

Dongyu Xu *is a Professor in the School of Civil Engineering and Architecture at the Linyi University. He received his BSc and MSc at University of Jinan, and obtained his PhD at Shandong University. His research interests are in cement based materials, smart materials and sensors, and structural health monitoring. He has published over 50 refereed research journal articles. His research has been recognized by National Technical Invention Award of China.*

Shoude Wang *is a Professor in the Shandong Key Laboratory of Building Materials Preparation and Testing Technology at the University of Jinan. He obtained his PhD at Wuhan University of Technology. His research interests are in cement and concrete material. He has published over 30 refereed research journal articles.*

Peng Du *is an associate Professor in the Shandong Key Laboratory of Building Materials Preparation and Testing Technology at the University of Jinan. He obtained his PhD at China Building Materials Academy. His research interests are in cement and concrete material. He has published over 20 refereed research journal articles.*

Publisher's Note: Engineered Science Publisher remains neutral with regard to jurisdictional claims in published maps and institutional affiliations.